Catalysis Science & Technology

ROYAL SOCIETY OF CHEMISTRY

PAPER

View Article Online
View Journal | View Issue

Cite this: *Catal. Sci. Technol.*, 2025, **15**, 1157

Partial framework-Al in lamellar H-[Al]-RUB-18: acidity by probe TMPO adsorption and catalytic study in the presence and absence of water†

Paulla B. F. Sousa, [ab] Elise M. Albuquerque,[b] Marco A. Fraga *[bc] and Heloise O. Pastore*[a]

While framework-Al (Al_{Td}) sites on [Al]-RUB-18 materials with Brønsted acidity were active in ethanol dehydration, the acidity of partial framework-Al sites (Al_{Oh} or aluminol sites) remains unknown. ^{31}P-MAS-NMR of adsorbed trimethylphosphine oxide (TMPO) was used together with catalytic reactions, in the presence and absence of water, to elucidate the acidity features of aluminol sites on lamellar RUB-18. Herein, spectroscopic analysis indicates that the ^{31}P signals arise from TMPO adsorbed on the lamella surface of RUB-18 ($\delta_{^{31}P}$ = 40–49 ppm), silanol/aluminol sites ($\delta_{^{31}P}$ = 49–56 ppm), and Brønsted acid sites (60–75 ppm). The crystallinity degree of the structure, Si/Al and Al_{Td}/Al_{Oh} molar ratios, and TMPO loadings, under wet and dry conditions, all lead to changes in ^{31}P resonances. Two resonance signals at 64 ppm and 69 ppm were attributed to partial and complete framework-Al sites, respectively. A clear correlation between the adsorption capacity of the active sites and peak intensities in the BAS region proves the influence of water in the adsorption process. This study brings additional evidence that the $(SiO_4)_4Al$ and $(SiO_4)_3Al–(OH)(H_2O)_2$ species played a crucial role in biomass-derivative conversion reactions. The simultaneous activity of Brønsted/Lewis acid sites was revealed, with the possibility of the $(SiO_4)_3Al–(OH)(H_2O)_2$ sites acting as LAS. The present study clarifies the acidity features of aluminol sites on lamellar [Al]-RUB-18 and brings attention to the evaluation of solid catalysts under aqueous-phase conditions.

Received 24th October 2024,
Accepted 9th January 2025

DOI: 10.1039/d4cy01288g

rsc.li/catalysis

Introduction

The lamellar silicate Na-RUB-18 is built by the union of [5^4] cavities that consist of four 5-membered rings of tetrahedral SiO_4. Lamella surfaces display silanolate/silanol groups; the interlamellar space is filled by hydrated Na^+ charge-compensating ions, which, by sharing edges, form 1-dimensional parallel chains in the [100, 010] directions.[1,2] The potential to chemically modify the framework of layered silicates increases the possibility of applications.[3,4] The isomorphous substitution (IS) of Si^{4+} by T^{3+}-atoms, such as Al^{3+} ions through hydrothermal synthesis, generates acid sites without changing their structure. The acidic properties of lamellar solids are created which endow the structure with new functionalities, with application in heterogeneous catalysis.[5–8]

[Al]-RUB-18 materials were prepared only recently,[9–13] therefore, their acidic properties are not yet completely known, especially concerning the correlation with the structure and composition of the lamella when compared with zeolites, their 3D-analogues. Lamellar aluminosilicates possess active catalytic sites exposed in the interlamellar space and on the surface of the crystals. Due to the easy access to the interlayer space, they can be enlarged by intercalation of bulky molecules.[11,14] Thus, these 2D materials have distinct advantages over zeolitic materials.

Many gas-phase reactions using acidic solid catalysts have been investigated and successfully employed by the chemical industry.[15] Most heterogeneous catalytic processes are conducted under elevated temperature and pressure conditions, where water is absent. However, active sites acting in liquid-phase transformations, where H_2O is the final product, the solvent, or still part of the biomass, are not completely understood.[16] The hydrothermal stability of the active sites in solid acid catalysts has become increasingly important in the few last years, and aqueous-phase biomass transformations require catalyst design strategies to avoid deactivation and improve durability.[17]

[a] *Micro and Mesoporous Molecular Sieves Group (GPM^3), Institute of Chemistry, University of Campinas, 13083-862 Campinas, SP, Brazil. E-mail: lolly@unicamp.br*

[b] *Laboratory of Catalysis, Instituto Nacional de Tecnologia (INT), 20081-312 Rio de Janeiro, RJ, Brazil. E-mail: marco.fraga@int.gov.br*

[c] *Department of Chemical and Materials Engineering, Pontifical Catholic University of Rio de Janeiro (PUC-Rio), 22453-900 Rio de Janeiro, RJ, Brazil*

† Electronic supplementary information (ESI) available. See DOI: https://doi.org/10.1039/d4cy01288g

Special attention is given to the need for water-tolerant acid sites in aqueous phase transformations over heterogeneous catalysts. In this regard, alternative chemical routes are researched for the use of bio-renewable and low-cost feedstocks. The residual biomass, originating from industry and as agriculture waste, is an alternative, renewable, and abundant carbon source.[18,19] In this context, hydrolysis of biopolymers that constitute biomass has emerged as a promising sustainable energy source to produce fuels and fine chemicals, reducing the global economy's reliance on fossil fuels.[20,21] In general, alkyl levulinates have attracted much attention due to their wide applications as chemical solvents, flavourings, and fuel additives.[22–24] Lactic acid (LA) is an important chemical compound for many industries, mainly related to its use in food additives and the production of biodegradable polymers (PLA – poly(lactic acid)).[25] Thus, lignocellulosic biomass is a promising route for obtaining furfuryl alcohol (FFA) to produce ethyl levulinate (EL).[24,26] Additionally, trioses are converted into lactic acid (LA), also using an aqueous phase system.[27–29] Moreover, aqueous-phase systems represent an effective and environmentally sustainable medium for biomass conversion.[30]

In this way, the incorporation of Al^{3+} ions into the lamellar framework ends up generating different Al species, such as framework-Al (tetrahedrally coordinated aluminum – Al_{Td}) and partial framework-Al sites (octahedrally coordinated aluminum – Al_{Oh} as aluminol sites or $(SiO_4)_3$–Al(OH)$(H_2O)_2$).[10] Such species could form different active acid sites on the lamella surface. It was proved that these acidic lamellar aluminosilicates contain aluminum structural sites (Al_{Td} sites) with Brønsted acidity, and these sites are active in the ethanol dehydration reaction.[11,13,31] Nevertheless, these reactions were conducted in the gas phase, and the acidic properties of [Al]-RUB-18, mainly aluminol sites, in the presence of water still remain to be fully evaluated.

Several analytical techniques were applied to characterize acid properties in catalyst solids: Hammett acid–base titration, microcalorimetry, thermo-programmed desorption of ammonia (TPD-NH_3), Fourier-transform infrared spectroscopy of acid-site adsorbed pyridine (FTIR-Py), and solid-state nuclear magnetic resonance spectroscopy.[32–35] Some experimental techniques do not allow complete acid characterization of the solid catalysts (nature, concentration, strength, and location of acid sites).[32]

However, solid-state ^{31}P-NMR gives quantitative and qualitative evaluations of Brønsted/Lewis acidity. This technique is based on the adsorption of trisubstituted phosphines or phosphine oxides, as probe molecules on acid sites.[35,36] It has been widely employed because ^{31}P is a naturally abundant nucleus (100%), with high sensitivity in the interactions between the probe molecules and active sites.[37–42] The ^{31}P-NMR spectra give information about the strength, nature, concentration, and spatial distribution/accessibility of the active sites (inside of the pores or on the surface of the crystals) by linear correlation with the chemical shifts, the peak positions, the spectrum/peak integration, and by using different probe molecule sizes, respectively.[43] Trimethylphosphine oxide (TMPO – M.P. = 140 °C) is extensively used in this process due to its kinetic diameter (0.55 nm) allowing adsorption on many catalysts, especially on microporous solids.[44] Also, this phosphine oxide (proton affinity = 910 kJ mol^{-1}) is a base with intermediate force when compared with other probe molecules applied in the measurements of acid properties, such as pyridine (proton affinity = 930 kJ mol^{-1}) and ammonia (proton affinity = 854 kJ mol^{-1}).[45] The advantageous aspect of this technique is its capacity to facilitate analysis in the presence and absence of water, adjust temperature treatments, and avoid damaging the structure of the catalyst.

In this study, the TMPO adsorption on H-[Al]-RUB-18 was performed in the presence and absence of water. Subsequently, solid-state ^{31}P-MAS-NMR spectroscopy of the phosphine oxide adsorbed as a probe molecule was applied to the structural evaluation of the partial framework-Al acidity on H-[Al]-RUB-18. Furthermore, the "active acidity" of the lamellar materials was also probed by using model reactions for the conversion of biomass derivatives. The activity and strength of the Brønsted acid sites (BAS) were evaluated using the alcoholysis reaction of FFA to produce EL.[46] Additionally, a continuous flow aqueous-phase reaction system was used to evaluate only the Lewis acid site (LAS) activity and the simultaneous activity of BAS and LAS. This involved the corresponding catalytic reactions: pyruvaldehyde conversion to LA[47] and the cascade reaction of dihydroxyacetone to form LA.[48]

Experimental

Syntheses of acidic lamellar silicate and aluminosilicates RUB-18

The analytical grade reactants employed in synthesis procedures were amorphous silica (silica-fumed, powder, 0.2–0.3 μm, Sigma-Aldrich), sodium hydroxide (pellets, 98% purity, Sigma-Aldrich), aluminum isopropoxide (98% purity, Alfa Aesar), and distilled water.

The silicate and aluminosilicate materials were synthesized according to the literature,[9,10] with modifications. A sodium metasilicate solution (Na_2SiO_3, molar composition: 0.05 SiO_2 : 0.10 NaOH : 1.31 H_2O) was prepared by dissolving NaOH in distilled water, followed by the addition of silica under magnetic stirring at 22 °C for 15 min. The well-dispersed suspension was transferred to a Teflon-lined stainless-steel autoclave and heated for 24 h at 100 °C. Silica (0.16 mol) was slowly added to the total volume of Na_2SiO_3 solution and kept under mechanical stirring at 22 °C for 60 min. The homogeneous, viscous, and bright gel (molar composition 0.05 Na_2SiO_3 : 0.16 SiO_2 : 1.36 H_2O) was completely transferred to a stainless-steel autoclave lined with Teflon® and hydrothermally treated in an oven for 14 days at 100 °C. The products (named Na-R18) were

washed with distilled water, filtered until neutral pH, and dried in the oven for 12 h.

The post-synthesis method to incorporate Al^{3+} on lamellar silicates (nominal Si/Al molar ratio = 15, 30, 60) was applied sequentially.[10] In the hydrothermal treatment step, it is essential to maintain a proportion of 77.8% of the volume used for NaOH solution concerning the capacity of the autoclave for synthesis reproduction (*e.g.*, 7 g of RUB-18 to 70 mL of 0.1 mol L^{-1} NaOH solution in an autoclave with a total capacity of 90 mL). The final products were named Na-[Al*x*]-R18, with *x* as the Si/Al experimental ratio.

The ion exchange procedures[13] were carried out by dispersing sodium lamellar materials in a 0.06 mol L^{-1} HCl solution (J.T. Baker, 36.5–38.0% w/w), maintaining the proportion of 0.0473 L g^{-1}, with magnetic stirring at room temperature (22 °C) for 30 min. The samples were filtered and washed with distilled water until a negative test for chloride ions using $AgNO_3$ was obtained. The products (H-[Al*y*]-R18, with *y* as the experimental Si/Al molar ratio) were dried in the oven for 12 h.

Structural and compositional characterization

The samples were analyzed by powder X-ray diffraction (XRD) on a Shimadzu diffractometer (XRD7000 model, CuKα radiation, λ = 1.54 Å, voltage 40 kV, current of 30 mA, detector SSD160-1D, inlet scattering slits of 1 mm), in a range of 2θ = 5° to 50° and at a scan rate of 0.5° 2θ min^{-1}.

The experiments of solid-state 1D-MAS-NMR were carried out with a Bruker Avance II^+ 400 MHz spectrometer using high power decoupling (HPDEC, B_0 = 9.4 T, with 10 kHz rotation at 22 °C, probe 2R, Zr rotor of 4 mm). The ^{29}Si-NMR spectra were obtained at a resonance frequency of 79.459 MHz, π/2 pulse (3.5 μs), and 60 s delay, using kaolinite as the reference. The ^{27}Al-NMR spectra were obtained at a resonance frequency of 104.261 MHz, π/12 pulse (1.25 μs), and 2 s delay, using aqueous acid $Al(NO_3)_3$ as the reference.

The elemental analyses were performed by X-ray fluorescence (XRF) on a Shimadzu (XRF 1800 model, Rh tube, 40 kV and 95 mA). The scan rate was 8° min^{-1} in a range of 10° to 140° using a diffraction crystal of LiF and a detector FPC to lightweight elements ($Z \leq 21$). The quantification of the elements was performed by the fundamental parameter protocol.

The Na element was quantified by inductively coupled plasma optical emission spectrometry (ICP-OES). The dissolution of the samples was carried out according to the methodology defined by ref. 49. The ICP-OES analyses were performed on a Perkin Elmer spectrometer (Optima 8300 model), with the following operating conditions: 1.3 kW power, a plasma gas flow rate of 0.5 L min^{-1}, λ^{-1} = 589.592 nm of emission line and axial viewing for the Na element.

Thermogravimetric (TG) and differential analyses (DTG) were performed using a SETSYS Evolution SETARAM. The samples (~14 mg) were heated in a flow of N_2 (16 mL min^{-1}), at a heating rate of 10 °C min^{-1} from room temperature to 1000 °C.

Evaluation of acidic properties in the presence and absence of water

TMPO adsorption experiments and solid-state ^{31}P-MAS-NMR spectroscopy. TMPO adsorption experiments were carried out in the following steps.[42,43] A portion of 300 mg of acid lamellar solids was placed into a Schlenk tube (see Fig. S1†) and connected to a vacuum line. The samples were heated up to a certain temperature (according to TG/DTG data – Fig. S2 and S6†) for 15 h to remove physisorbed water and other impurities. For the analysis in the presence of water, the re-hydration procedure was applied in the same Schlenk under vacuum, heating another cell with a calculated mass of $CoCl_2{\cdot}6H_2O$ (Sigma-Aldrich) at 140 °C for 90 min. The mass of water in the hydrated metallic complex was equivalent to the proportion of 2 : 1 mol of H_2O to Al_{Oh} sites based on each Al content in acidic lamellar solids. Further experiments were conducted in selected samples to saturation with physisorbed H_2O, by the respective TG/DTG data. A specific volume of 54.3 mmol L^{-1} of $(CH_3)_3PO/CH_2Cl_2$ solution (TMPO – Alfa Aesar/CH_2Cl_2 solvent – Synth, 99.5% anhydrous) was used for each sample, adjusted to achieve different TMPO loadings (P/Al molar ratio = 1.4, 1.2, 0.50 and 0.25). Afterwards, this portion of the solution and 30 mL of CH_2Cl_2 were added to the sample in a dry glovebox under an argon atmosphere. The suspension was maintained for 1 h in the sealed Schlenk, after which the Schlenk tube was again connected to the vacuum line to remove the solvent, at 50 °C for 1 h. Following that, the TMPO@sample was treated at 165 °C for 1 h to ensure uniform diffusion and distribution of the probe molecules on the active sites. Finally, the Schlenk was opened in a dry glovebag under argon and the TMPO@sample was packed into a MAS-NMR zirconia rotor (ø = 4 mm), and sealed with a gas-tight Kel-F cap. The high-power decoupling (HPDEC) ^{31}P-MAS-NMR spectra were obtained at a resonance frequency of 161.9 MHz (Bruker Avance II^+ 400 MHz, with 10 kHz at 22 °C), a pulse of π/2 (1.931 μs), a delay of 20 s and 5400 scans, using concentrated H_3PO_4 as the reference. Lorentz deconvolution spectral analysis results are shown as red dashed curves, and the asterisks denote spinning sidebands in the graphs.

Additional characterization of acidic properties: catalytic model reactions to convert biomass derivatives

Reaction in batch process. The alcoholysis reaction of furfuryl alcohol (FFA) was performed in a batch multi-reactor at 150 °C for 3 h, under 15 bar N_2 pressure.[46] For that, 0.029 g of each H-[Al]-R18 catalyst was added to the reactors with 5 mL of 0.2 mol L^{-1} FFA (Sigma-Aldrich, 98% purity) solution in ethanol (EtOH, Sigma-Aldrich, anhydrous, <0.003% de H_2O; extra-pure absolute). Previously, inert gas was used to purge the system. The reactors were then sealed, and pressure and temperature were adjusted. Time and magnetic stirring were counted after the system reached the desired temperature. Products were collected at the end of the reaction, filtered with PTFE filters (22 μm),

quantified, and analyzed on an Agilent Technologies gas chromatograph using a flame ionization (GC-FID, model 7890B) or a mass spectrometer (GC-MS) detector. The method of GC-MS analysis is found in the ESI.† In CG-FID, the products were separated using an HP-Innowax column (30 m × 530 μm × 1 μm), with a 1 mL min^{-1} N_2 flow and a heating ramp from 80 °C to 240 °C. The inlet temperature was 280 °C, with 1 μL injection volume in triplicate, a 10 : 1 split ratio, and 11 mL min^{-1} total flow.

Reactions in the continuous flow system. The conversions of 1,3-dihydroxyacetone (DHA, dimer, Sigma-Aldrich, 97% purity) and pyruvaldehyde (PA solution, 40% wt in H_2O, Sigma-Aldrich) to lactic acid were performed in a fixed-bed continuous flow reaction system in aqueous medium.[47,48] A 0.2 mol L^{-1} substrate solution was pumped at a flow rate of 0.3 mL min^{-1} using an HPLC Gilson 307 pump. A back pressure Swagelok valve maintained a pressure of 10 bar in the system. A 316 stainless steel reactor ($ø_{inner}$ = 4.15 mm) was heated at the desired temperature (130 °C). The H-[Al]-R18 catalyst (300 mg, h_{bed} = 7 cm, and τ = 9 min) was secured with quartz wool at the inlet and outlet of the reactor. Products were collected in a time range of the reaction, filtered with PTFE filters (22 μm), quantified, and analyzed on a high-performance liquid chromatography system (HPLC), using an Agilent Technologies 1110 instrument equipped with a refractive index detector (RID) at 50 °C. Aliquots of 5 μL were injected in triplicate, and the products were separated on an HPX-87H column at 65 °C, with a flow of 0.7 mL min^{-1} of 5 mmol L^{-1} H_2SO_4 solution as the mobile phase.

Equations for catalytic performance. All compounds were identified based on their respective retention times. Substrate conversion (X_r), product selectivity (S_p), and carbon balance (CB) were determined by eqn (1) to (3), respectively:

$$X_r = \left(\frac{[r_0] - [r_t]}{[r_0]}\right) \cdot 100\% \quad (1)$$

$$S_p = \left(\frac{n \cdot [p_t]}{n \cdot [r_0] - n \cdot [r_t]}\right) \cdot 100\% \quad (2)$$

$$CB = \left(\frac{n \cdot [r_t] + \sum n \cdot [p_t]}{n \cdot [r_0]}\right) \cdot 100\% \quad (3)$$

where n is the number of carbon atoms in the molecule, $[r_0]$ is the initial concentration of the reactant, and $[r_t]$ and $[p_t]$ are the concentrations of the reactant and products at time (t), respectively.

Results and discussion

Structural characteristics of lamellar materials

The chemical compositions of acidic samples are summarized in Table S1.† The partial substitution of Si^{4+} to Al^{3+} ions on the RUB-18 structure is indicated by the final Si/Al molar ratios for the products and the 90–99% ion exchange efficiency.

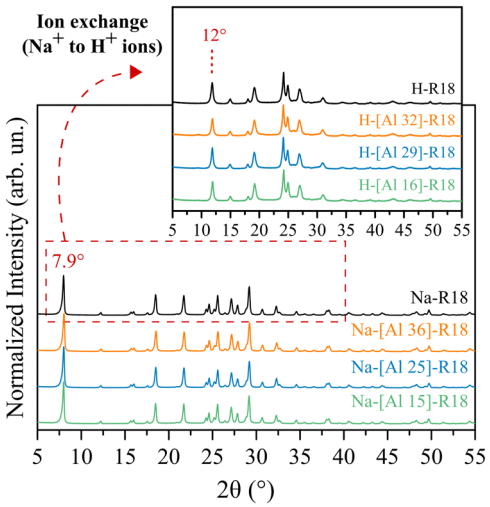

Fig. 1 XRD patterns for sodium and acidic lamellar RUB-18, with different Si/Al molar ratios. Inset: zoomed image of a Bragg angle region.

The structural properties of the lamellar silicate and aluminosilicate materials are displayed in Fig. 1 and 2. XRD patterns (Fig. 1) for sodium samples show a peak at around 2θ = 7.9° corresponding to the basal space of the lamella in the c direction [004] (d_{004} = 1.1 nm). The peak range from 2θ = 15° to 35° characterizes the crystalline structure of Na-RUB-18.[9,10] Amorphization of the structure, indicated by a halo in the range between 20 and 30° 2θ, was not observed. There were some changes in the relative intensities and shifted peaks, but a unique crystalline phase was observed in the samples prepared in this work. The removal of hydrated interlamellar cations $[Na(H_2O)_6]^+$ from the interlayer spaces caused the appearance of a typical intrinsic structural order for H-RUB-18,[50] and reduced the interlayer space. The diffractograms indicate that the basal space in H-RUB-18 is 0.74 nm (peak at 2θ = 12°).

According to the ^{29}Si-MAS-NMR spectra (Fig. 2A), two resonance signals at −99 ppm and −111 ppm are visualized. These signals are characteristic of Q^3 [$(SiO_4)_3$–Si–(OH)/$(SiO_4)_3$–Si–O–Na^+] and Q^4 [$(SiO_4)_4$–Si] type-Si^{4+} sites found in the Na-RUB-18 structure, respectively, Fig. 2B.[1,9,10,51] The larger presence of silanol/silanolate groups, given by the highest signal intensity of the Q^3 sites, suggests structural defects and smaller crystal sizes than standard RUB-18 (Q^3/Q^4 ratio = 1).[2,10] Moreover, only slight changes in peak shapes (height and width) were observed after Al insertion demonstrating that the presence of Al in the structure did not cause order disturbances in these samples. Contrarily, peak broadening and variation in the intensity of the resonance signals were observed for the H-[Al]-R18 samples. These features demonstrate changes in the local order of sites, probably indicating different angles of T–O–T bonds for Si^{4+} species

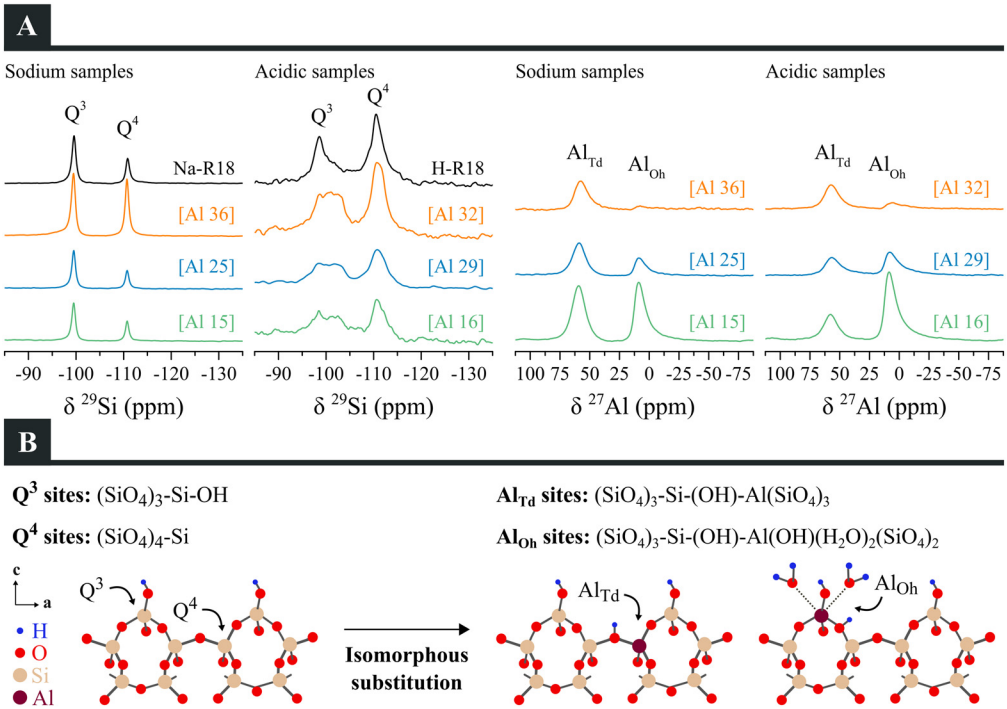

Fig. 2 (A) ^{29}Si- and ^{27}Al-MAS-NMR spectra for sodium and acidic lamellar RUB-18, with different Si/Al molar ratios. [Aly] are the aluminosilicate catalysts with *y* equal to the experimental Si/Al molar ratio. (B) Graphical representation of the Si^{4+} and Al^{3+} species on a structural unit of RUB-18 (cavities [5^4] in [101] directions): silanol groups as Q^3 sites; siloxane groups as Q^4 sites; complete framework-Al as Al_{Td} sites; and partial framework-Al or hydrated aluminol species as Al_{Oh} sites.

upon Al introduction and ion exchange. In addition, a small resonance signal at −101 ppm is attributed to Si(3Si, 1Al) species.[52] A decrease in the Q^3/Q^4 ratio in the H-[Al]-R18 samples in relation to Na-[Al]-R18 was observed, which depends on the aluminum concentration in the materials (see Table S1† for details).

The formation of Al_{Td} and Al_{Oh} species and the influence of Q^3 sites in the IS process on the RUB-18 structure were verified by ^{27}Al-MAS-NMR analysis. As illustrated in Fig. 2A, the peaks corresponding to tetrahedral (Al_{Td}) and octahedral (Al_{Oh}) aluminum sites for the Na- and H-[Al]-R18 samples were observed at *ca.* 60 ppm and 8 ppm, respectively.[51] It was shown before that framework (Al_{Td}) and partial-framework (Al_{Oh}) Al species in the RUB-18 structure correspond to $(SiO_4)_4Al$ and $(SiO_4)_3Al–(OH)(H_2O)_2$ species (Fig. 2B), respectively.[13,53] The coordination of water in aluminol sites was already observed in sodium lamellar aluminosilicate RUB-18 and confirmed by DFT calculations.[13,53] The combination of variations in the Q^3 site content and the IS results in fluctuations of Al_{Td} to Al_{Oh} species concentrations. A higher content of Al_{Td} species was found when reducing the total Al content (Na-[Al36]-R18 sample), resulting in better dispersion of these species on the lamellar structure. In contrast, an increase in Al_{Oh} in relation to Al_{Td} species was noted due to a higher Al content on the RUB-18 lamellar surface (Na-[Al15]-R18 sample). The ^{27}Al-MAS-NMR spectra of acidic solids exhibited analogous characteristics to those observed in sodium materials. However, the Al_{Td} sites decreased in comparison with the peaks for aluminol sites, Al_{Oh}. This finding suggests that the ion exchange method induced partial hydrolysis of the Al–O bonds, which led to the Al(Td) → Al(Oh) transformation.[54] The final Al_{Td}/Al_{Oh} ratios of acidic non-seeded samples prepared in this work are reported in Table S1.†

It is essential to understand the type of acid site (AS) formed on the lamellar surface of RUB-18, particularly that originating from aluminol sites, and if the AS becomes more or less acidic or even loses activity under wet conditions. Furthermore, the presence of a large number of silanol/aluminol groups in the RUB-18 structure makes it difficult to determine the acidity properties at elevated temperatures. Given this information, the subsequent characterization was conducted to appropriately assess the acidity of H-[Al]-RUB-18 lamellar solids.

Acidity properties analyzed by ^{31}P-MAS NMR

Evaluation of ^{31}P chemical shifts of TMPO adsorbed on RUB-18. In light of the aforementioned results and the data published,[10–13] the isomorphous substitution process of Si^{4+} to Al^{3+} atoms in the RUB-18 structure occurs on the lamellar surface. As a result, Al species were formed in tetrahedral (Al_{Td}) and octahedral (Al_{Oh}) coordinations. Typical Brønsted acid sites (BAS) originate from one acidic proton introduced in the form of Si–O(H)–Al groups, also

called bridging –OH, for each substituted framework (Al_{Td} sites) or partial-framework atom (Al_{Oh} or aluminol sites).[13] In this way, the adsorption experiments were conducted with TMPO as a probe molecule because it is more sensitive to the strength of BAS than LAS in solid acid catalysts.[35] The chemical shift range to the reaction products of TMPO with BAS is $\delta_{^{31}P}$ = 50–100 ppm;[44] the larger the chemical shift, the stronger the acidity. The mark of 86 ppm has been assigned as the threshold for superacidity.[36] Between 50 ppm and 60 ppm, the peak could be indicative of LAS in zeolites[40,41] or –SiOH internal/external groups in zeolites without LAS.[42]

The ^{31}P-MAS-NMR spectra of the dehydrated samples with different Si/Al and P/Al molar ratios are shown in Fig. 3. No resonance signals were visualized at 31 ppm and 39 ppm associated with mobile and crystalline TMPO.[41] This is indicative that the probe molecules were physisorbed and chemisorbed with $\delta_{^{31}P}$ values of around 40–49 ppm and 50 ppm to 80 ppm, respectively.[44]

As seen in Fig. 3A, the spectrum with high TMPO loading (P/Al ratio = 1.20) for acidic lamellar silicate exhibits one resonance signal. The symmetric and thin peak at 44 ppm is relative to the physisorbed TMPO.[43] The crystallinity pattern for the H-R18 sample guarantees the homogeneous adsorption of probe molecules on the lamella surface. The rise of resonance signals in the BAS region proves the insertion of Al in framework positions of RUB-18, with chemical shift values in the region between $\delta_{^{31}P}$ = 60 and 80 ppm. Thus, four signals were visualized for the three spectra of acidic aluminosilicate samples (H-[Al]-R18, with Si/Al ratios = 32, 29, and 16). The presence of the Al in the RUB structure causes an upfield shift in the $TMPO_{(Phys.)}$ signal to 41 ppm. Also, the appearance of a small resonance peak at *ca.* 49 ppm could be attributed to TMPO complexes interacting with ≡SiOH/≡AlOH on the surface and edges of the lamella. The increase in the content of aluminol sites (Al_{Td}/Al_{Oh} molar ratio = 3.38 to 0.45) leads to a downfield shift ($\delta_{^{31}P}$ = 52 ppm) and a rise in intensity of this peak. The peaks above *ca.* 60 ppm identified as the $TMPOH^+$ ions formed by the interaction of TMPO with BAS. Moreover, the narrowing and shifting of this chemisorbed signal can be explained by the uniform distribution of Al_{Td} species on the lamella surface. Therefore, the reduction of Al concentration facilitates the insertion of stronger BAS into the structure of the solid.[36,41]

The adsorption of TMPO with P/Al molar ratio = 0.5 in dehydrated acidic samples is shown in Fig. 3B. The reduction of the TMPO concentration allowed a better resolution of the signals. This is reflected in the intensity of the signals when the physisorbed peak decreases and the other ones increase accordingly. No resonance signal was identified in the spectrum of silicate H-R18 (Si/Al = ∞). One explanation for this phenomenon is that the adsorption process in these materials occurs first in stronger acid sites, the BAS, and only when they are filled, the physisorption occurs and H-R18 presents no strong acid sites.[43]

Equivalent results were obtained for the H-[Al]-R18 samples (Si/Al = 32 and 29), whereby only medium to strong intermolecular interactions were observed in the spectrum. For the H-[Al16]-R18, the amount of TMPO solution was doubled as a function of the increased Al concentration, thus the expected physisorption signal was observed at 44 ppm. The small peak characteristic of TMPO adsorbed on ≡SiOH/≡AlOH sites was shifted from *ca.* 49 ppm to around

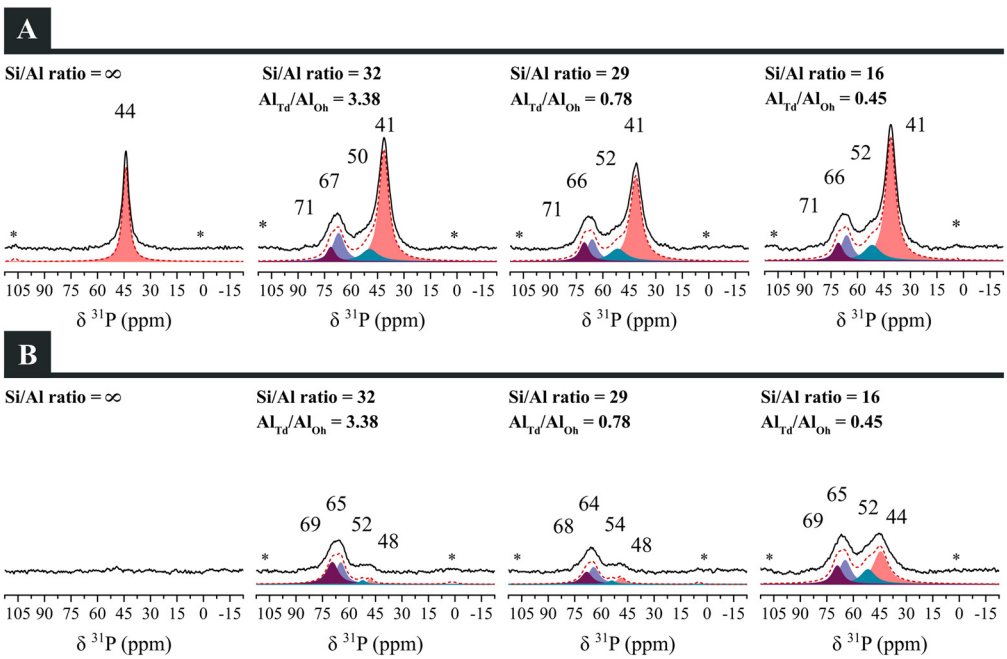

Fig. 3 ^{31}P-MAS-NMR spectra for H-R18 and H-[Al]-R18 non-seeded samples in the absence of water, with different Si/Al and Al_{Td}/Al_{Oh} molar ratios and P/Al molar ratios equal to (A) 1.20 and (B) 0.50.

52–54 ppm. This downfield-shifted peak at *ca.* 52 ppm can be explained by the interactions of the ≡SiOH groups that make the chain-connected groups *via* hydrogen bonds; see discussion about FTIR spectra in the Summary of spectroscopic analysis of Al-sites section.

The results of TMPO interaction with a BAS in low TMPO concentration were identified by the two peaks at *ca.* 64 ppm and 69 ppm. It is known that the peak positions in the spectrum are indicative of the varying strengths of BAS.[36,55] Overall, the peak at 69 ppm becomes more intense with low total aluminum content, and consequently, with a high Al_{Td}/Al_{Oh} molar ratio (sample with Si/Al ratio = 32 and Al_{Td}/Al_{Oh} ratio = 3.38), in accordance with the presence of stronger BAS. Table S2† exhibits the variation in signal percentages in the BAS region for dehydrated samples with P/Al molar ratio = 0.50 when changing the Si/Al ratio. Bornes *et al.*[41] identified changes in the ^{31}P-NMR spectra of HZSM-5 by probing TMPO with P/Al ratios = 0.21 to 0.75. According to these authors, the percentage of spectral intensity in the Brønsted region varied with changes in the TMPO content. Also, the BAS resonance signals identified by the authors at around $\delta_{^{31}P}$ = 64–87 ppm arise from the confinement effect of protonated TMPO in HZSM-5 pores.

Additional TMPO analysis in lamellar seeded RUB-18 materials: proof of concept. The following discussion pertains to lamellar samples synthesized with seed crystals. Experimental data about long/short-range structural ordering for acidic seeded materials are found in the ESI† (Fig. S3 to S6†).

According to Wright,[56] high supersaturation and the seeding technique made it possible to control the final products, including the distribution of crystals' sizes. This resulted in the production of crystallites that were significantly smaller in size.[56] Thus, the excess of ≡SiOH sites on the lamellar surface is caused by the diminishing of crystallite size. In parallel, the formation of aluminol species (Al_{Oh}) in high concentrations is favoured. The ^{27}Al- and ^{29}Si-NMR spectra for sodium and acidic lamellar samples are displayed in Fig. S5.† The final Al_{Td}/Al_{Oh} molar ratios of Al species in solids were: 0.35 for H-[Al47]-R18$_{(seeded)}$ and 0.15 for H-[Al25]-R18$_{(seeded)}$.

Furthermore, the ion exchange process, followed by ammonia thermo-decomposition to afford the acid samples, resulted in variations of diffraction patterns that are characteristic of the RUB-18 structure as seen in Fig. S3.† The fluctuations of intensity, broadening of the peaks, and reduction in the signal/noise ratio are all in agreement with previous studies of H-RUB-18 prepared with this procedure.[11] Despite the partial amorphization of the structure, the absorption range between 1300 cm^{-1} and 400 cm^{-1} in the FTIR spectra shows that the structural units of the RUB have been preserved after the calcination step (Fig. S4†),[9] thus the local organization of the sites is intact.

The partial framework-coordinated Al species (aluminol sites) on seeded RUB-18 were also probed by the TMPO ^{31}P-MAS-NMR spectroscopy technique (Fig. 4).

When the samples are saturated with TMPO (P/Al molar ratio = 1.4), the physisorbed probe molecules on the lamella

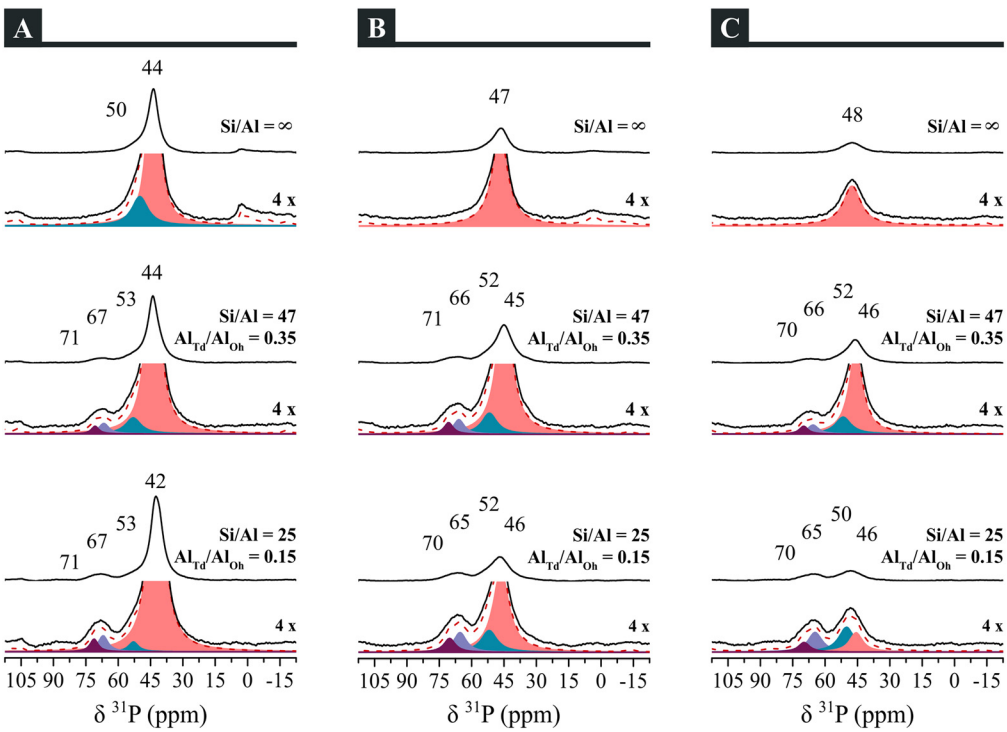

Fig. 4 ^{31}P-MAS-NMR spectra for H-R18 and H-[Al]-R18 seeded samples in the absence of water, with different Si/Al and Al_{Td}/Al_{Oh} molar ratios and P/Al molar ratios = (A) 1.4, (B) 0.50, and (C) 0.25. The deconvoluted signals were magnified 4×.

surface are also seen in the spectra by the peak at 42–44 ppm. In addition, the small resonance shoulder appeared in the spectra at 50–53 ppm even for the silicate H-R18$_{(Seeded)}$ sample. The small crystal size, thus the abundant external surface, and the large content of ≡SiOH groups all confer distinct strengths of interaction between the adsorbate and active sites. Hence, the chemical environment of the ^{31}P nucleus is changed, which is reflected in the position and shape of the signals in the spectrum.

In relation to the non-seeded synthesis, the higher the Al_{Oh}/aluminol concentration and/or the less crystalline the structure both observed in seeded samples, the higher will be the signal corresponding to ≡SiOH and ≡SiOH/≡AlOH: it goes from $\delta_{^{31}P}$ = 49–52 ppm in non-seeded aluminosilicate samples to 50–53 ppm on the seeded silicate and aluminosilicate ones. Also, two peaks were again observed above 60 ppm, for all TMPO concentrations (P/Al ratio = 1.40 to 0.25). These BAS peaks arise from $TMPOH^+$ species. In summary, the spectroscopic analysis of non-seeded H-[Al]-R18 samples (see Fig. 3) can be used to explain the behavior of adsorption sites and chemical shift values for ^{31}P obtained for acidic seeded solids.

Influence of water in the adsorption process and spectroscopic analysis. TMPO is prone to deliquescence and, consequently, the standard procedure requires a dehydration step before the adsorption process.[44] However, an alternative approach to study the "invisible acid nature" using the trimethyl phosphine and phosphine oxide ^{31}P-NMR technique is to conduct experiments on dehydrated and partially hydrated probe-loaded samples and compare the spectra.[57,58]

In the present study, the influence of water was investigated to further clarify the acid site behavior. The experiments were initially conducted with 2 : 1 mol of H_2O to aluminol sites (Al_{Oh}). The initial idea is to create the initial hydrated Al_{Oh} sites and analyze the effects on the acidity of these sites. The spectra for H-[Al]-R18 samples with low TMPO loading and different Si/Al ratios are presented in Fig. 5.

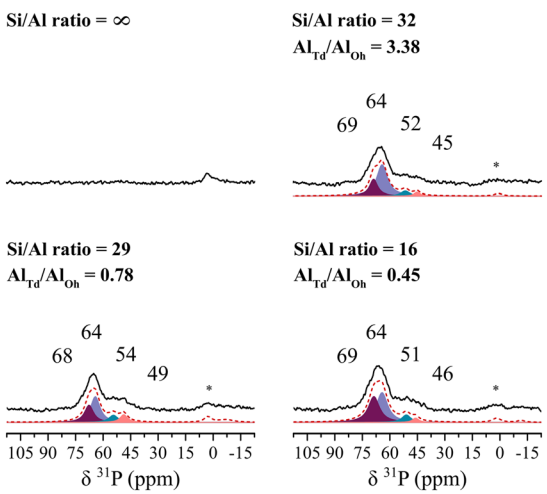

Fig. 5 ^{31}P-MAS-NMR spectra for H-R18 and H-[Al]-R18 non-seeded samples in the presence of water (2 mol H_2O : 1 mol Al_{Oh}), with different Si/Al and Al_{Td}/Al_{Oh} molar ratios, and P/Al molar ratio = 0.50.

As expected, all aluminosilicate lamellar solids present a decline in the intensity of the TMPO$_{(Phys.)}$ signal in relation to the signals associated with chemisorbed TMPO above $\delta_{^{31}P}$ = 60 ppm. This is more evident in the H-[Al16]-R18 spectrum by comparison to its dehydrated spectrum (see Fig. 3B and the signal's percentage in Table S2†). As illustrated in the lamellar silicate spectrum, H_2O molecules do not affect the ≡SiOH groups in the sense of favouring probe molecule adsorption. However, the aluminosilicate spectra indicate that the peak at *ca.* 64 ppm is significantly enhanced in intensity, even concerning the peaks at *ca.* 68 ppm (see Table S2† and comparison of hydrated and dehydrated non-seeded samples with P/Al = 0.50). These experimental results provide information on the identity of the Al species, in which the $\delta_{^{31}P}$ = 64 ppm and 68 ppm signals could be associated with partial framework-Al sites and complete framework-Al sites, respectively.

Supplementary experiments to simulate the saturated environment with water/adsorbent were performed in seeded samples and H-[Al16]-R18 (Fig. 6). Upon exposure to humidity, the samples with high TMPO concentration had shifted peaks at $\Delta\delta_{^{31}P}$ = 1–2 ppm and an increase in the relative intensity of these signals in the spectra (Fig. 6A).

Moreover, an evident reduction in the TMPO$_{(Phys.)}$ signal is accomplished with an intensity increase of BAS signals in the H-[Al16]-R18 sample (Fig. 6B). When the P/Al ratio was reduced in the same H_2O saturated environment (Fig. 6C), the BAS for H-[Al47]-R18$_{(seeded)}$ (Al_{Td}/Al_{Oh} ratio = 0.35) retained their acidic features (peaks at $\delta_{^{31}P}$ = 66–71 ppm). A similar acidic behavior is observed in H-[Al16]-R18 (Al_{Td}/Al_{Oh} ratio = 0.45), even for P/Al molar ratio = 0.50 and H_2O/Al_{Oh} molar ratio = 2 (Fig. 5). Published studies[59,60] confirm the existence of ≡Si–O–H···(–O)–Si≡ bridges that form a network of hydrogen bonds on the lamella surface, as well as enable the dynamics and conduction of protons in this region as a function of temperature variation. Thus, the peak values displayed indicate large H-bond interactions of probe molecules with these sites in an environment saturated with H_2O molecules, resulting in the considerable deshielding of ^{31}P resonances to downfield.

In general, TMPO adsorption analysis in aqueous media suggests the maintenance of acid sites, easing the interactions of the probe molecules with the RUB-18 structure. The activity of these sites was not adversely affected, in other words, there was neither total deactivation nor loss of acidity in the presence of water. Contrarily, this solvent favoured the interactions of the probe molecules with the acid sites in the RUB-18 structure. The coordination of H_2O molecules to aluminol sites, or even by saturation with water, enhances both acidity and the adsorption capacity of the acid sites. This finding suggests that these sites in the lamellar material could be used in aqueous-phase catalytic reactions, as already shown for H-[Al]-magadiite.[14]

Summary of spectroscopic analysis of Al-sites. Many authors have extensively studied experimental and

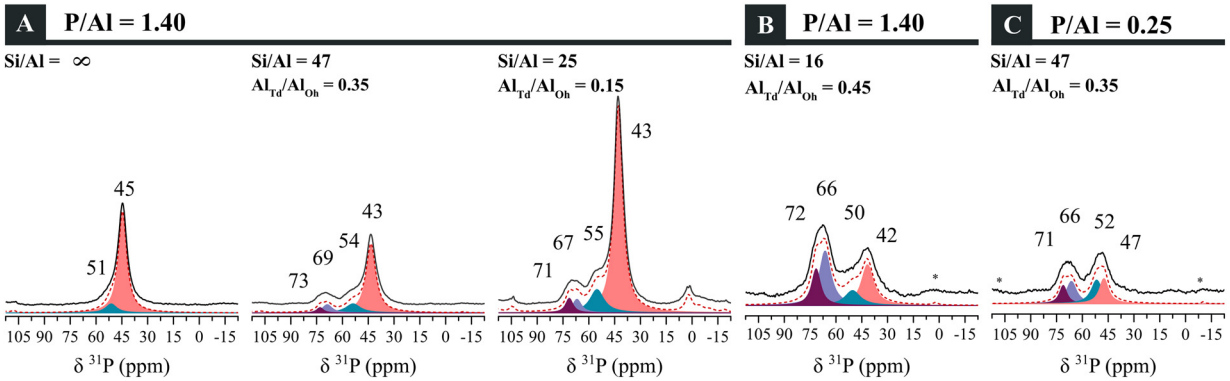

Fig. 6 ^{31}P-MAS-NMR spectra for hydrated materials, saturated with physisorbed H_2O molecules: (A) H-R18 and H-[Al]-R18 seeded samples, with different Si/Al and Al_{Td}/Al_{Oh} molar ratios, and P/Al molar ratio = 1.40; (B) H-[Al16]-R18 and (C) H-[Al47]-R18$_{(seeded)}$ samples, with different TMPO loadings (P/Al molar ratio). The deconvoluted signals for (B) and (C) graphs were magnified 3× concerning (A) graphs.

computational modeling to probe acid site distributions in various solid acid catalysts, principally in zeolites.[44] In our study, the absence of channels and cavities simplifies the attribution of configuration modes of TMPO adsorbed on RUB-18 based on the existent information about zeolites.

Despite the existence of information on zeolites, the resonance signals as a function of the typical lamellar structure are not completely clarified by the literature. An alternative approach is exploring the data from TMPO adsorbed on MCM-41,[36,61] BEA,[42,62] and H-ZSM-5.[63,64] The goals are to identify the TMPO resonance signals observed in spectra and to establish a correlation between the RUB-18 structure with the mesoporous/microporous structures that contain few signals at the same $\delta_{^{31}P}$ region, ≡SiOH groups, and BAS/LAS in different proportions, and the same structural unit (cavities [5^4]).

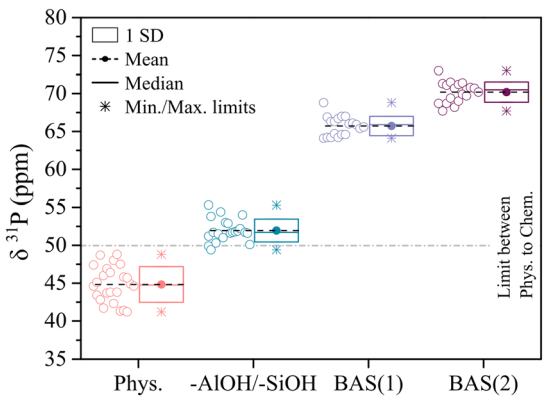

Fig. 7 Boxplot of $\delta_{^{31}P}$ (ppm) values for TMPO adsorbed over non-seeded and seeded lamellar RUB-18 as a function of the following possible site types: physisorbed TMPO (○ – light red), –AlOH/–SiOH groups (○ – dark cyan), BAS(1) from partial framework-Al species (○ – light purple), and BAS(2) from complete framework-Al species (○ – purple). The box represents one standard deviation (SD) according to the distribution of the values. The gray dash-dotted line is the limit of molecular interactions (Chem. = chemisorption, and Phys. = physisorption).

Thus, the spectroscopic analysis by ^{31}P-NMR gave us interesting information about acidic features, mainly structural–activity correlation in lamellar solid acid catalysts. Notably, we have observed the influence of some factors that can change resonance peak positions and intensities (height and width). These factors are as follows: the crystallinity degree of the structure, the amount of aluminum (Si/Al molar ratios), complete and partial framework-Al species (Al_{Td}/Al_{Oh} molar ratios), adsorption under wet or dry conditions, and varying TMPO loadings.

Fig. 7 displays the distribution of the dataset relative to the chemical shift values of the ^{31}P nucleus of the resonance signals from non-seeded and seeded lamellar materials. Overall, three main regions of the $\delta_{^{31}P}$ (ppm) were identified with TMPO adsorption modes, with one of them containing a subgroup: physisorbed TMPO (40–50 ppm), TMPO strongly adsorbed on ≡SiOH/≡AlOH and possible LAS (50–60 ppm), and TMPO interacting with Brønsted acid sites (60–80 ppm) from partial, BAS(1), and complete, BAS(2), framework-Al species.

White and coworkers[65] investigated post-synthetic treatments in ZSM-5 and identified second tetrahedrally coordinated Al sites. One such site is $(SiO)_3$–Al(OH) species, designated as Al(IV)-2 as illustrated in Fig. 4(b) of ref. 65. These species correspond to the BAS(1) sites when the partial framework-Al sites are dehydrated, which are schematized in our work as shown in Fig. 2B. According to these authors, other $(SiO)_{4-n}$–Al$(OH)_n$ species are formed from Al(IV)-2 sites using the typical dealumination process.[65] Additionally, White and coworkers[65–68] examined the MFI catalyst frameworks to ascertain details regarding the spatial proximity between the Al(IV)-1 and Al(IV)-2 sites, the synergy of these paired active sites, and the post-synthesis modifications that led to an enhancement in the catalytic activity of HZSM-5 through the use of water.

It is important to show that the presence of aluminol sites from partial framework-Al species is also indicated by the interaction of its hydroxyl group with the neighboring silanol sites by H-bonding. For that, FTIR of the pure lamellar

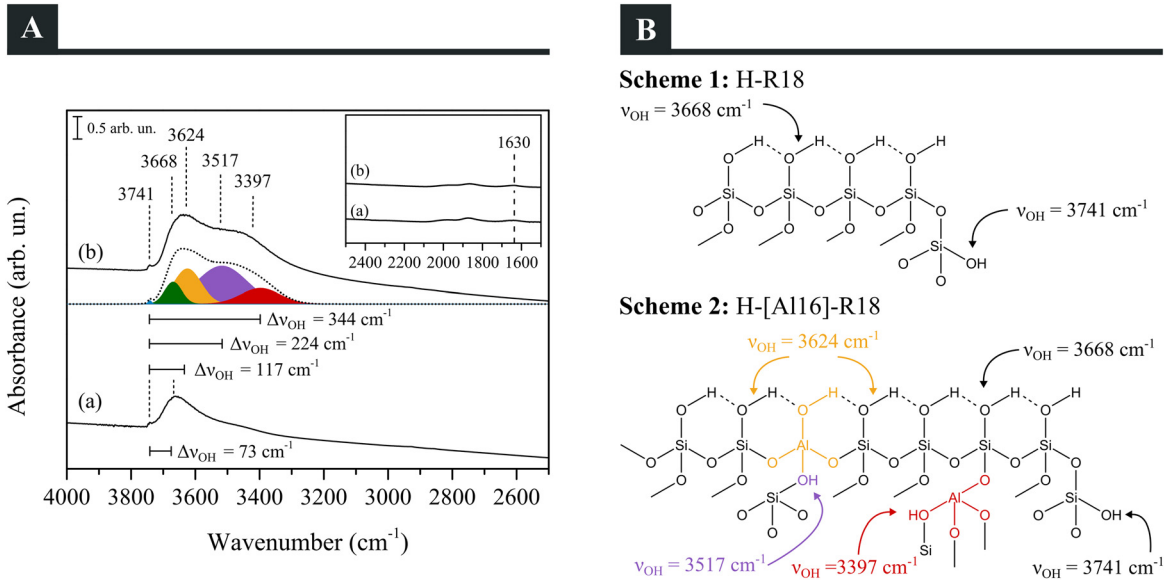

Fig. 8 (A) FTIR spectra for pure dehydrated (a) H-R18 and (b) H-[Al16]-R18 non-seeded samples. Inset: FTIR spectra region within 2500–1500 cm^{-1}. (B) Schemes of a chain of H-bonds on the lamella surface of H-R18 and H-[Al16]-R18 non-seeded samples in the [010] direction.

silicate was used in comparison with aluminosilicate. Fig. 8 shows the result.

The samples were dehydrated at 350 °C for 15 h under high vacuum (~10–6 mmHg). The FTIR spectra shown in Fig. 8A (insert) demonstrate, by the absence of peaks in the 1630 cm^{-1} region, that the samples are dehydrated. The profile in the region from 3800 cm^{-1} to 3000 cm^{-1} is the one typical of silicates and zeolites and was also observed in H-magadiite and in H-[Al]-magadiite.[6]

The first point to call attention is that, despite the absence of water, the bands in the high-frequency region are broad. This is the typical consequence of extensive H-bonding. The H-bonding displaces the OH stretching vibration to lower wavenumbers, the displacement is proportional to the proton transfer to the atom that is making the H-bond, that is, the more basic the atom with which the proton is shared or the more acidic the proton, the larger the displacement. In the same line, the larger will be the vibration molar absorptivity, ε.[69] The result is that the bands are shifted to lower wavenumbers and increase in intensity.

The spectrum in Fig. 8A, curve (a), shows one very low intensity band at 3741 cm^{-1}, due to a minute concentration of isolated Si–OH groups.[6] In the cases where these groups are really isolated, the band is very narrow, and at approximately the same position. The more intense band at 3668 cm^{-1} corresponds to the OH vibration of SiOH involved in a chain of H-bonds, as indicated in Fig. 8B, Scheme 1. The frequency difference, $\Delta\nu_{OH}$, is only 73 cm^{-1}, indicating a small proton displacement.

The addition of aluminum to the RUB-18 structure causes changes in the FTIR curve, Fig. 8A(b). The bands observed in H-RUB-18 are still present; the sample presents a small amount of isolated SiOH groups and the chain of H-bonded SiOH groups. Because of that, the bands at 3741 and 3668 cm^{-1} are still present. However, as was discussed in this work, there will be aluminol, AlOH, groups, isolated bridging acid sites, ≡Si(OH)Al≡, and acidic groups neighboring aluminol sites. Besides these, H-bonded silanol groups that neighbor aluminol sites will be disturbed by them and are expected to appear to be slightly shifted. The slightly disturbed SiOH will show a slightly larger displacement from the isolated SiOH than the purely H-bonded SiOH, thus the band at 3624 cm^{-1} can be caused by this effect, the $\Delta\nu_{OH}$ is 117 cm^{-1}, and the presence of the Al atom causes the H on SiOH to be more acidic in that situation.

Naturally, the largest displacement will be that of the band at 3397 cm^{-1}, which corresponds to the isolated, bridging acid site, the ≡Si(OH)Al≡ group (in red, Scheme 2, Fig. 8B), and in this case, the $\Delta\nu_{OH}$ is 344 cm^{-1} in relation to the isolated Si–OH. Finally, the acidic groups neighboring aluminol sites, in purple, Scheme 2 in Fig. 8B, will appear between the two bands; this is the cause of the elevated baseline. A band at around 3517 cm^{-1} is suggested as the result of the presence of this group; it would afford a $\Delta\nu_{OH}$ of 224 cm^{-1} in relation to the isolated silanol group. The acidity of this group is situated between that of the proton in SiOH in the chain of silanol groups disturbed by the presence of Al–OH (in orange, Scheme 2 in Fig. 8B) and that of the isolated acidic site in red, Scheme 2 in Fig. 8B.

Each one of these groups corresponds to a peak of TMPO NMR spectra (Fig. 3A), the TMPO adsorbed in SiOH/AlOH at 52 ppm corresponds to the band at 3624 cm^{-1}, the acid site at the aluminol groups adsorbs TMPO and shows a peak at 66 ppm that appears at 3517 cm^{-1} and finally, the

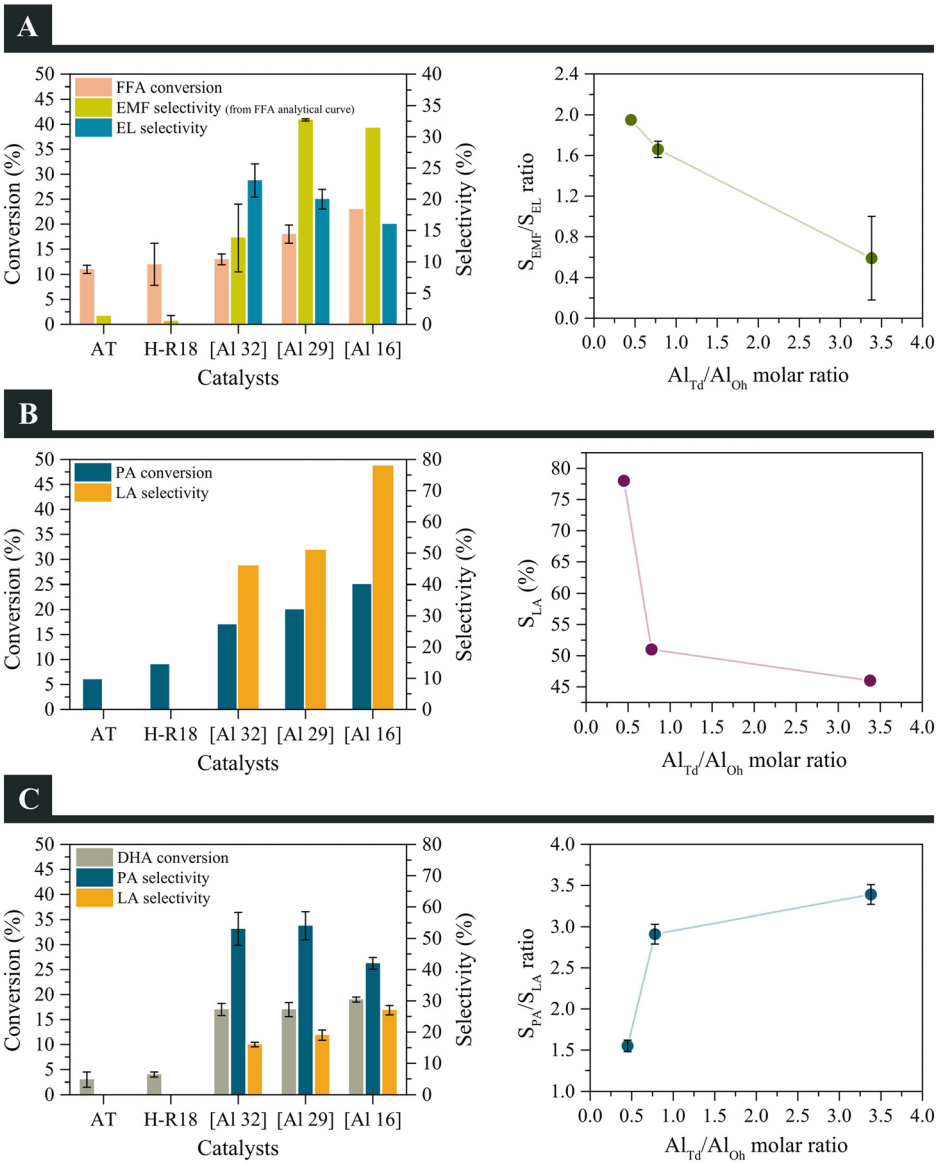

Fig. 9 Conversion (*X*, %) and selectivity (*S*, %) values, and respective graphs of the relationship between structural properties and selectivity ratios for H-[Al]-R18 catalysts: (A) alcoholysis of FFA (3 h of reaction), (B) PA reactions (values for 3 h of reaction), (C) hydrolysis of DHA (average values for 3 h and 6 h of reaction). Carbon balance (CB) was determined within the range of 86–96%, based on measurements obtained through CG-FID and HPLC-RID techniques. In the "Catalysts" axis, the autothermal reactions are represented by AT, and [Al*y*] are the aluminosilicate catalysts with *y* equal to the Si/Al molar ratio before the reaction.

most acidic site, the isolated ≡Si(OH)Al≡ adsorbs TMPO and causes a ^{31}P chemical shift of 71 ppm and a FTIR band at 3397 cm^{-1}.

Catalytic tests

Strength of BAS through the batch process. The results of the alcoholysis of furfuryl alcohol (FFA) to form ethyl levulinate (EL) are shown in Fig. 9A. Autothermal reactions or those using non-acidic catalysts (H-R18) have a small contribution to FFA conversion. It was observed that FFA conversion increased when the reaction was catalyzed over lamellar aluminosilicate samples with a larger Al content. The selectivity values to both products increased as the Al content increased (Si/Al = 32 to 16).

EL and 2-ethoxymethyl-furan (EMF) have been identified after 3 h of reaction, while the conventional hydrolysis products, angelica lactones and levulinic acid, were not detected. GC-MS was used to confirm these products (method in the ESI†). A reaction pathway for EL and EMF production that requires BAS with medium strength is proposed in Fig. S7.†

Fig. 9A demonstrates the relationship between the structural properties of the catalysts and the ratio between EMF and EL selectivity. The selectivity for EL is enhanced when the Al_{Oh} content is reduced, and the Si/Al ratio is increased in the catalysts. According to the literature,[70–73] the

ethanolysis of FFA could occur in two steps depending on the catalysts used. The first step involves BAS and/or LAS for the etherification of FFA. The second step involves the hydrolysis of EMF over BAS with higher strength to form EL. Li and collaborators[72] confirmed the dependence on the strength/nature of the active sites in ethanolysis reactions catalyzed over ZSM-5 with different Si/Al ratios. Strong sites with the highest BAS/LAS ratio produce more EL than EMF compared to catalysts with the lowest strength of sites and BAS/LAS ratio.

Thus, the partial Al-framework and framework-Al species in the RUB-18 structure played a crucial role in this reaction. The H-[Al16]-R18 sample exhibited greater selectivity towards EMF. In contrast, the selectivity to EL was correlated with a higher concentration of Al_{Td} species and a relative medium strength of Brønsted acid sites in the H-[Al32]-R18 sample. These results are in line with previous studies on zeolites[70–73] and evidence the activity of H-[Al]-R18 as Brønsted acid catalysts as foreseen from the acidity characterization.

Activity of BAS and/or LAS through the continuous flow aqueous-phase system. The transformation of pyruvaldehyde (PA) into lactic acid (LA) is a typical Lewis acid-catalyzed reaction.[27,47] The results are presented in Fig. 9B. The blank experiments revealed that AT and H-R18 had a negligible contribution to PA conversion, and LA was not even identified as a product in these reactions. On the other hand, all H-[Al]-R18 catalysts were active, disclosing the Lewis activity of these lamellar solids, and consistently, selectivity to LA. It is worth mentioning that in the presence of water, the TMPO adsorption also revealed the concentration increase in the Lewis acid sites (compare Fig. 3B with Fig. 6B and C). The more acidic catalyst (H-[Al16]-R18, with a lower Si/Al ratio) showed a selectivity to LA above 75%.

The PA conversion and LA selectivity increase with the higher concentration of Al_{Oh} species and the lower Si/Al ratio. The relationship between the LA selectivity and Al_{Td}/Al_{Oh} molar ratios of the catalysts can be seen in Fig. 9B. The results state that the presence of Al in the octahedral coordination as aluminol sites in the RUB-18 structure influenced the reaction pathway. The reactions catalyzed by H-[Al32]-R18 and H-[Al29]-R18 have comparable LA selectivity.

For this reason, it is suggested that partial framework-Al sites (Al_{Oh} as aluminol sites) in the RUB-18 catalyst structure behaved as Lewis acid sites. In Fig. 10, the proposed reaction pathway follows the coordination of the pyruvaldehyde on Al, in Al_{Oh} sites, instead of, or displacing, H_2O molecules, forming a cyclic intermediate. The H_2O molecules in the reactional medium act as nucleophiles and proton donors for the Cannizzaro reaction in a concerted mechanism. It is important to indicate that the H_2O molecules are continuously re-coordinated to the Al site, thereby recovering these acid sites.[27]

According to Albuquerque and co-workers,[47] there is a correlation between the strength of the acid sites and the reaction rate. The authors noted that medium-strength sites are the minimal requisite for the Cannizzaro reaction. Therefore, it can be inferred that the H-[Al]-R18 samples contain medium strength Lewis acid sites needed to cause the intramolecular rearrangement of pyruvaldehyde to form lactic acid.

BAS are required for the dehydration step of DHA to form PA, and the intramolecular rearrangement of PA to form LA only occurs *via* LAS.[48] This reaction was used as another continuous aqueous-phase transformation to evaluate the simultaneous activity of the BAS and LAS over silicate and aluminosilicate catalysts (Fig. 9C).

The blank experiments presented low conversions, and thus their PA selectivity, or selectivity to any other organic compound, could not be assertively quantified. Catalysts H-[Al]-R18 were active to convert DHA, with 17–19% ± 2% conversion. The PA and LA were the main products. The presence of pyruvaldehyde (PA) proves the insertion of BAS in the RUB-18 structure, corroborating the initial results in furfuryl alcohol alcoholysis. The dehydration of DHA resulted in an increased PA selectivity, ΔS_{PA}, of 12% when the Si/Al ratio was increased, from 42% to 54%.

Lactic acid (LA) was also produced in the next step as could be anticipated from the reaction runs using pyruvaldehyde as a feedstock. As commented, Lewis acid sites are required to promote the Cannizzaro mechanism and transform PA into LA. The following final selectivity values were ~16% to ~27% when the Si/Al ratio of the catalysts was decreased from 32 to 16. Therefore, as in the case of FFA and PA conversion reactions, the intrinsic relationship between the products' selectivity and the catalysts' structural properties was observed once again. As seen in Fig. 9C, a

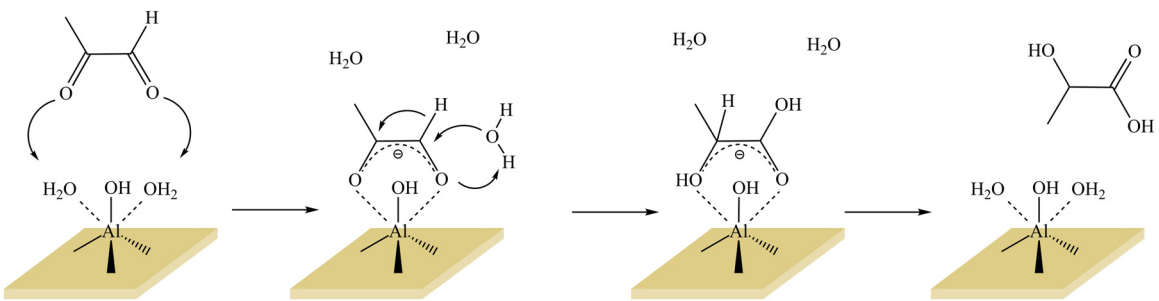

Fig. 10 Illustration of pyruvaldehyde adsorption by displacement of water molecules on hydrated aluminol sites (as Lewis acid sites) in the lamellar surface of H-[Al]-RUB-18.

higher concentration of Al_{Oh} sites results in a considerable consumption of PA to form LA. Thus, H-[Al16]-R18 is the best catalyst among the ones prepared in this work for the DHA into LA transformation *via* the cascade reaction. Meanwhile, H-[Al32]-R18 is a better acidic solid that promotes the first step reaction, with high PA selectivity.

These findings reinforce the hypothesis that the aluminol, $(SiO_4)_3Al–(OH)(H_2O)_2$, sites in the RUB-18 structure act as LAS in the aqueous phase reactions. Furthermore, the X_{DHA}, S_{PA}, and S_{LA} values remained constant during the investigated reaction timeframe, indicating an effective simultaneous activity of BAS and LAS, and that these lamellar catalytic systems are stable.

The structural properties of H-R18 and H-[Al]-R18 catalysts before and post-PA and DHA reactions are discussed below and summarized in Table S3.† The XRD pattern (Fig. S8†) indicates that the long-range structural order characteristic of H-RUB-18 was preserved. For the H-R18 sample, peaks at 2θ = 13° and 26° suggest the presence of residual quartz wool recovered from the reactor with the catalyst. A slight broadening of the baseline was observed at around the 2θ = 15° to 30°, which might also be attributed to residual wool. Moreover, a slight reduction in the intensity of the peaks above 2θ = 20° indicates a possible partial loss of the crystalline structure for RUB-18.

The ^{27}Al-NMR analysis (Fig. S9†) shows a modification of the short-range structural order. An increase in the peak area relative to Al_{Oh} species and a reduction of the Al_{Td} content for both reactions were observed. Partial hydrolysis of Al–O bonds has been considered. If the conversion and selectivity values and the structure by the XRD pattern are kept, the variation can be related to the creation of $(SiO_4)_3Al(OH)(H_2O)_2$ species. As a result, the BAS activity is not eliminated. Also, the LAS activity in aluminol sites is maintained. Fig. S10† shows the tendency of variation in the Al species concentration as a function of the initial Al concentration for each catalyst. For DHA reactions, the positive $\Delta[Al_{Oh}]$ and negative $\Delta[Al_{Td}]$ confirm the transformation of the species without loss of structural Al. On the other hand, the negative Δ[total Al species] detected after PA reaction indicates the loss of the Al framework of the structure.

Summary of catalyst reactivity

It is also clear that the catalysts exhibit BAS/LAS acidity, which affords the interactions between the substrate (FFA, DHA, PA) and acid sites on the RUB-18 lamellar surface. Higher selectivity and conversion were observed in aqueous-phase transformations, in which the acidity behavior arises from an H_2O and substrate-saturated environment. These results are consistent with the results of the ^{31}P spectra discussed in Fig. 6. Some authors have proposed several types of LAS, such as framework LAS from tri-coordinate aluminum, extra-framework (EFAL with an octahedral coordination), and framework-associated aluminum (Al_{Td} to Al_{Oh} reversible coordination).[54,62,74,75] According to the authors,[54] the latter type becomes kinetically allowed and thermodynamically stable under wet conditions, allowing for a reversible transition between BAS and coordinatively saturated LAS. Thus, these authors propose that three water molecules in the 1st coordination shell are firmly bound to partial framework-Al_{Oh} in $Al(SiO_3)_3(H_2O)_3$ arrangement.[54]

Our study, contrarily, suggests that the partial framework-Al species is $(SiO_4)_3–Si–(OH)–Al(OH)(H_2O)_2(SiO_4)_2$ sites (or aluminol sites – Al_{Oh}, as seen in Fig. 2B) on the lamella surface of RUB-18. It contains two water molecules and one OH group directly bound to Al. This hydroxyl is the one that disturbs the H-bonded SiOH chain as seen in the FTIR spectra. Such sites could be assigned either as Brønsted and/or Lewis acid sites, depending on the experimental conditions used. Brønsted acidity is the only one found in an anhydrous environment without coordinating reactants while Lewis acidity will also be present, together with the Brønsted one, in the presence of water or any coordinating solvent or reactant.

Conclusions

A larger concentration of silanol/silanolate groups influenced the isomorphous substitution process that occurs on the lamellar silicate surface of RUB-18, with a direct correlation between the Si/Al molar ratio in the synthesis and the aluminum species in the structure. The present work shows that the experiments carried out using the ^{31}P-NMR technique on dehydrated and hydrated TMPO-loaded samples in combination with catalytic tests provide new insights into the acidic properties of partial framework-Al sites on non-seeded and seeded H-[Al]-RUB-18.

This work shows that some factors lead to changes in ^{31}P-NMR resonances, such as the crystallinity degree of the structure, the amount of aluminum in the sample (Si/Al ratio), the presence of complete and partial framework-Al species, adsorption under wet or dry conditions, and varying TMPO loadings. The spectroscopic analysis of the ^{31}P nucleus indicates that the resonance signals arise from TMPO adsorbed on silanol groups ($\delta_{^{31}P}$ = 40–49 ppm), silanol/aluminol sites ($\delta_{^{31}P}$ = 49–56 ppm), and Brønsted acid sites (60–75 ppm). In lower TMPO concentrations, the spectral data revealed at least the existence of two types of BAS with different strengths at *ca.* 64 ppm and 68–69 ppm. Upon exposure to humidity, the coordination of water molecules to aluminol sites enhanced the TMPO adsorption capacity of the active sites. This resulted in an increase in the resonance peak intensities, for both the Al_{Td} and Al_{Oh} species, associated with the peaks at 69 and 64 ppm, respectively. A water and TMPO-saturated environment induced changes in the signals above 50 ppm, both in the position and intensity, implying that no loss of acidity, and possibly no deactivation, occurs in the presence of water. This would result in enhanced catalytic activity when subjected to similar experimental conditions.

The "active acidities" of the H-[Al]-R18 lamellar non-seeded samples were tested in both batch and flow systems in the presence and absence of water. It is worth noting that the $(SiO_4)_4Al$ and $(SiO_4)_3Al–(OH)(H_2O)_2$ species present in the RUB-18 structure played a crucial role in biomass-derivative conversion reactions. The H-[Al32]-R18 catalyst has a better performance in producing ethyl levulinate in the ethanolysis reaction and pyruvaldehyde in DHA dehydration. This is attributed to the uniform distribution of Al_{Td} species that are more isolated due to the smaller Al content in the RUB structure, which facilitates the insertion of stronger BAS. Conversely, the H-[Al16]-R18 catalyst exhibited a significant selectivity towards 2-ethoxymethyl-furan (an intermediate in the ethanolysis reaction). This indicates that the BAS are not sufficiently strong for complete 2-ethoxymethyl-furan hydrolysis. Finally, the production of lactic acid (the final product of DHA and PA conversions) over lamellar aluminosilicates RUB-18 under aqueous conditions reveals the possibility of the $(SiO_4)_3Al–(OH)(H_2O)_2$ sites (Al_{Oh} sites) acting as Lewis acid sites.

The ^{31}P-NMR spectroscopic analysis and catalytic test approach reinforce the improvement in acidity under wet conditions and highlight the acid behavior of partial framework-Al sites in the RUB-18 structure. This work initiates the effort to create a consistent protocol for acidity analysis in lamellar solids, comparable to the existing ones for zeolites, and brings the importance of evaluating the acidity characteristics of solid catalysts under aqueous-phase conditions.

Data availability

The data supporting this article have been included as part of the ESI.†

Author contributions

P. B. F. S. contributed to the investigation, validation, formal analysis, visualization, and writing – original draft. E. M. A. contributed to the methodology, supervision, validation, and writing – review & editing. M. A. F. contributed to the conceptualization, methodology, validation, resources, supervision, and writing – review & editing. H. O. P. contributed to the conceptualization, methodology, validation, resources, supervision, funding acquisition, project administration, and writing – review & editing.

Conflicts of interest

There are no conflicts to declare.

Acknowledgements

P. B. F. S. and H. O. P. acknowledge the Fundação de Amparo à Pesquisa do Estado de São Paulo (FAPESP – grant 2022/05743-0 for P. B. F. S., project no. 2021/12058-0) for the financial support to this work. E. M. A. (Proc. 405800/2022-3) thanks Conselho Nacional de Pesquisa Científica e Tecnológica (CNPq) for her post-doctoral grant. M. A. F. also acknowledges the Fundação de Amparo à Pesquisa do Estado do Rio de Janeiro (FAPERJ) for financial support (E-26-202.660-2019). H. O. P. thanks CNPq for the scholarship. Coordenação de Aperfeiçoamento de Pessoal de Nível Superior (CAPES) – Financial Code 001 is also acknowledged. Also, the authors thank the LIRMN (IQ-UNICAMP) for the NMR analyses, Dr. Erica Munsignatti (GMP^3/UNICAMP) for all her experimental support in the development of this work, and Dr. Vinícius W. Faria (INT) for his experimental support in the catalytic tests using furfuryl alcohol.

References

1 S. Vortmann, J. Rius, S. Siegmann and H. Gies, *Ab initio* structure solution from X-ray powder data at moderate resolution crystal structure of a microporous layer silicate, *J. Phys. Chem. B*, 1997, **101**, 1292–1297.
2 M. Borowski, O. Kovalev and H. Gies, Structural characterization of the hydrous layer silicate Na-RUB-18, $Na_8Si_{32}O_{64}(OH)_8·32H_2O$ and derivatives with XPD-, NPD-, and SS NMR experiments, *Microporous Mesoporous Mater.*, 2008, **107**(1–2), 71–80.
3 T. Sirinakorn, K. Imwiset, S. Bureekaew and M. Ogawa, Inorganic modification of layered silicates toward functional inorganic-inorganic hybrids, *Appl. Clay Sci.*, 2018, **153**, 187–197.
4 T. Selvam, A. Inayat and W. Schwieger, Reactivity and applications of layered silicates and layered double hydroxides, *Dalton Trans.*, 2014, **43**, 10365.
5 G. L. Paz, E. C. O. Munsignatti and H. O. Pastore, Novel catalyst with layered structure: Metal substituted magadiite, *J. Mol. Catal. A: Chem.*, 2016, **422**, 1–8.
6 G. B. Superti, E. C. Oliveira, H. O. Pastore, G. Gatti and L. Marchese, Aluminum Magadiite: an Acid Solid Layered Material, *Chem. Mater.*, 2007, **19**, 4300–4315.
7 Y. Ide, N. Kagawa, M. Sadakane and T. Sano, Precisely designed layered silicate as an effective and highly selective CO_2 adsorbent, *Chem. Commun.*, 2013, **49**, 9027.
8 N. Alam and R. Mokaya, Strongly acidic mesoporous aluminosilicates prepared via hydrothermal restructuring of a crystalline layered silicate, *J. Mater. Chem. A*, 2015, **3**, 7799.
9 F. S. O. Ramos, E. C. O. Munsignatti and H. O. Pastore, 2D–3D structures: The hydrothermal transformation of a layered sodium silicate, Na-RUB-18, into mordenite zeolite, *Microporous Mesoporous Mater.*, 2013, **177**, 143–150.
10 F. S. O. Ramos and H. O. Pastore, 2D-to-disguised 3D materials with built-in acid sites: H^+-[Al]-RUB-18, *Dalton Trans.*, 2017, **46**, 11728–11737.
11 G. P. Campos, G. B. Báfero and H. O. Pastore, Vapor adsorption experiments as a characterization tool for layered catalysts, *New J. Chem.*, 2020, **44**, 9998.
12 G. B. Báfero, E. C. O. Munsignatti and H. O. Pastore, Lamellar-zeolitic transformations mediated by diffusionless and recrystallization mechanisms, *Microporous Mesoporous Mater.*, 2021, **323**, 111189.

13 G. B. Báfero, B. N. N. Silva, A. A. Leitão and H. O. Pastore, The behavior of aluminum sites in H-[Al]-RUB-18 catalysts: A theoretical-experimental investigation, *Mol. Catal.*, 2023, **535**, 112870.
14 G. P. Campos, E. M. Albuquerque, M. A. Fraga and H. O. Pastore, Continuous Cellobiose Hydrolysis over Lamellar Aluminosilicates—Unveiling [Al]-magadiite Water-Tolerant Acid Sites, *Ind. Eng. Chem. Res.*, 2021, **60**(13), 4794–4805.
15 A. Corma, From Microporous to Mesoporous Molecular Sieve Materials and Their Use in Catalysis, *Chem. Rev.*, 1997, **97**(6), 2373–2420.
16 T. Ennaert, J. Van Aelst, J. Dijkmans, R. De Clercq, W. Schutyser, M. Dusselier, D. Verboekend and B. F. Sels, Potential and challenges of zeolite chemistry in the catalytic conversion of biomass, *Chem. Soc. Rev.*, 2016, **45**, 584–611.
17 J. Huo, J.-P. Tessonnier and B. H. Shanks, Improving Hydrothermal Stability of Supported Metal Catalysts for Biomass Conversions: A Review, *ACS Catal.*, 2021, **11**(9), 5248–5270.
18 R. A. Sheldon, Green chemistry, catalysis and valorization of waste biomass, *J. Mol. Catal. A: Chem.*, 2016, **422**, 3–12.
19 M. Niakan, C. Qian and S. Zhou, Highly Efficient One-Pot Conversion of Glucose to 5-Hydroxymethylfurfural over Acid-Base Bifunctional MCM-41, Mesoporous Silica under Mild Aqueous Conditions, *Energy Fuels*, 2023, **37**(21), 16639–16647.
20 A. Kruse and A. Gawlik, Biomass conversion in water at 330–410 C and 30– 50 MPa. Identification of key compounds for indicating different chemical reaction pathways, *Ind. Eng. Chem. Res.*, 2003, **42**(2), 267–279.
21 Y. B. Huang and Y. Fu, Hydrolysis of cellulose to glucose by solid acid catalysts, *Green Chem.*, 2013, **15**, 1095–1111.
22 D. Song, *et al.*, Efficient conversion of levulinic acid or furfuryl alcohol into alkyl levulinates catalyzed by heteropoly acid and ZrO_2 bifunctionalized organosilica nanotubes, *J. Catal.*, 2016, **333**, 184–199.
23 C. R. Patil, S. P. Kamble and C. V. Rode, Single-Pot Alcoholysis of Furfuryl Alcohol to Alkyl Levulinates Using Heterogenized p-TSA Catalyst, *ChemistrySelect*, 2021, **6**, 6636–6643.
24 S. H. Chung, S. de Haart, R. Parton and N. R. Shiju, Conversion of furfuryl alcohol into alkyl-levulinates using solid acid catalysts, *Sustain. Chem. Clim. Action*, 2022, **1**, 100004.
25 Y. J. Wee, J. N. Kim and H. W. Ryu, Biotechnological production of lactic acid and its recent applications, *Food Technol. Biotechnol.*, 2006, **44**(2), 163–172.
26 C. Antonetti, D. Licursi and S. Fulignati, *et al.*, New frontiers in the catalytic synthesis of levulinic acid: from sugars to raw and waste biomass as starting feedstock, *Catalysts*, 2016, **6**, 196.
27 K. M. A. Santos, E. M. Albuquerque, L. E. P. Borges and M. A. Fraga, Discussing Lewis and Brønsted acidity on continuous pyruvaldehyde Cannizzaro reaction to lactic acid over solid catalysts, *Mol. Catal.*, 2018, **458**(B), 198–205.
28 K. M. A. Santos, E. M. Albuquerque, G. Innocenti, L. E. P. Borges, C. Sievers and M. A. Fraga, The Role of Brønsted and Water-Tolerant Lewis Acid Sites in the Cascade Aqueous-Phase Reaction of Triose to Lactic Acid, *ChemCatChem*, 2019, **11**, 3054–3063.
29 E. M. Albuquerque, L. E. P. Borges and M. A. Fraga, Lactic acid production from aqueous-phase selective oxidation of hydroxyacetone, *J. Mol. Catal. A: Chem.*, 2015, **400**, 64–70.
30 A. H. Van Pelt, O. A. Simakova, S. M. Schimming, J. L. Ewbank, G. S. Foo, E. A. Pidko, E. J. M. Hensen and C. Sievers, Stability of functionalized activated carbon in hot liquid water, *Carbon*, 2014, **77**, 143–154.
31 R. K. S. Almeida, G. L. Paz, G. B. Báfero and H. O. Pastore, Properties of Layered [Al]- and [V,Al]-Magadiite Catalysts as Revealed by Ethanol Dehydration, *Microporous Mesoporous Mater.*, 2019, **284**, 1–9.
32 E. G. Derouane, J. C. Védrine, R. R. Pinto, P. M. Borges, L. Costa, M. A. N. D. A. Lemos, F. Lemos and F. R. Ribeiro, The Acidity of Zeolites: Concepts, Measurements and Relation to Catalysis: A Review on Experimental and Theoretical Methods for the Study of Zeolite Acidity, *Catal. Rev.: Sci. Eng.*, 2013, **55**, 454–515.
33 M. Niwa, N. Katada, M. Sawa and Y. Murakami, Temperature-Programmed Desorption of Ammonia with Readsorption Based on the Derived Theoretical Equation, *J. Phys. Chem. A*, 1995, **99**, 8812–8816.
34 M. Tamura, K. Shimizu and A. Satsuma, Comprehensive IR study on acid/base properties of metal oxides, *Appl. Catal., A*, 2012, **433–434**, 135–145.
35 A. Zheng, S. Liu and F. Deng, Acidity characterization of heterogeneous catalysts by solid-state NMR spectroscopy using probe molecules, *Solid State Nucl. Magn. Reson.*, 2013, **55–56**, 12–27.
36 A. Zheng, S.-J. Huang, W.-H. Chen, P.-H. Wu, H. Zhang, H.-K. Lee, L.-C. de Ménorval, F. Deng and S.-B. Liu, ^{31}P Chemical Shift of Adsorbed Trialkylphosphine Oxides for Acidity Characterization of Solid Acids Catalysts, *J. Phys. Chem. A*, 2008, **112**(32), 7349–7356.
37 J. Guan, X. Li, G. Yang, W. Zhang, X. Liu, X. Han and X. Bao, Interactions of phosphorous molecules with the acid sites of H-Beta zeolite: Insights from solid-state NMR techniques and theoretical calculations, *J. Mol. Catal. A: Chem.*, 2009, **310**(1–2), 113–120.
38 Y. Seo, K. Cho, Y. Jung and R. Ryoo, Characterization of the Surface Acidity of MFI Zeolite Nanosheets by ^{31}P NMR of Adsorbed Phosphine Oxides and Catalytic Cracking of Decal, *ACS Catal.*, 2013, **3**, 713–720.
39 C. Bornes, M. Sardo, Z. Lin, J. Amelse, A. Fernandes, M. Ribeiro, C. Geraldes, J. Rocha and L. Mafra, ^{1}H–^{31}P HETCOR NMR elucidates the nature of acid sites in zeolite HZSM-5 probed with trimethylphosphine oxide, *Chem. Commun.*, 2019, **55**(84), 12635–12638.
40 Y. Wang, S. Xin, Y. Chu, J. Xu, G. Qi, Q. Wang, Q. Xia and F. Deng, Influence of trimethylphosphine oxide loading on the measurement of zeolite acidity by solid-state nmr spectroscopy, *J. Phys. Chem. C*, 2021, **125**(17), 9497–9506.

41 C. Bornes, M. Fischer, J. Amelse, C. Geraldes, J. Rocha and L. Mafra, What Is Being Measured with P-Bearing NMR Probe Molecules Adsorbed on Zeolites?, *J. Am. Chem. Soc.*, 2021, **143**(34), 13616–13623.
42 D. Zasukhin, I. Kasyanov, Y. Kolyagin, A. Bulygina, K. Kharas and I. Ivanova, Evaluation of Zeolite Acidity by ^{31}P MAS NMR Spectroscopy of Adsorbed Phosphine Oxides: Quantitative or Not?, *ACS Omega*, 2022, **7**(14), 12318–12328.
43 X. Yi, H. Ko, F. Deng, S. Liu and A. Zheng, Solid-state ^{31}P NMR mapping of active centers and relevant spatial correlations in solid acid catalysts, *Nat. Protoc.*, 2020, **15**(10), 3527–3555.
44 D. Zasukhin, I. Kostyukov, I. Kasyanov, Y. Kolyagin and I. Ivanova, ^{31}P NMR Spectroscopy of Adsorbed Probe Molecules as a Tool for the Determination of the Acidity of Molecular Sieve Catalysts (A Review), *Pet. Chem.*, 2021, **61**(8), 875–894.
45 National Institute of Standards and Technology, *NIST Chemistry WebBook*, **https://webbook.nist.gov/chemistry/**, (Accessed: Feb 10, 2023).
46 V. W. Faria, K. M. A. Santos, A. M. Calazans and M. A. Fraga, Hydrolysis of Furfuryl Alcohol to Angelica Lactones and Levulinic Acid over Nb-based Catalysts, *ChemCatChem*, 2023, **15**, e202300447.
47 E. L. Albuquerque, L. E. P. Borges and M. A. Fraga, Relationship between Acid-Base Properties and the Activity of ZrO_2-Based Catalysts for the Cannizzaro Reaction of Pyruvaldehyde to Lactic Acid, *ChemCatChem*, 2017, **9**, 2675–2683.
48 K. M. A. Santos, E. M. Albuquerque, T. L. Coelho and M. A. Fraga, Continuous aqueous-phase cascade conversion of trioses to lactic acid over Nb_2O_5 catalysts, *Biomass Convers. Biorefin.*, 2023, **13**, 11865–11878.
49 F. S. O. Ramos, R. K. S. Almeida, C. A. Lopes Júnior, M. A. Z. Arruda and H. O. Pastore, A Straightforward Method for Determination of Al and Na in Aluminosilicates Using ICP OES, *J. Braz. Chem. Soc.*, 2017, **28**(8), 1–7.
50 M. Borowski, B. Marler and H. Gies, The crystal structure determination of the crystalline layered silicic acid H-RUB-18, *Z. Kristallogr.*, 2002, **217**, 233–241.
51 G. Engelhardt and D. Michel, *High-resolution Solid State NMR of Silicates and Zeolites*, Wiley, Chichester, 1987.
52 S. Mintova, V. Valtchev, T. Onfroy, C. Marichal, H. Knözinger and T. Bein, Variation of the Si/Al ratio in nanosized zeolite Beta crystals, *Microporous Mesoporous Mater.*, 2006, **90**(1–3), 237–245.
53 H. M. Moura, F. A. Bonk, R. C. G. Vinhas, R. Landersb and H. O. Pastore, Aluminium-magadiite: from crystallization studies to a multifunctional material, *CrystEngComm*, 2011, **13**, 5428–5438.
54 M. Jin, M. Ravi, C. Lei, C. Heard, F. Brivio, Z. Tošner, L. Grajciar and J. A. van Bokhoven, Dynamical Equilibrium between Brønsted and Lewis Sites in Zeolites: Framework-Associated Octahedral Aluminum, *Angew. Chem., Int. Ed.*, 2023, **62**, e202306183.
55 A. Zheng, S. B. Liu and F. Deng, ^{31}P NMR Chemical Shifts of Phosphorus Probes as Reliable and Practical Acidity Scales for Solid and Liquid Catalysts, *Chem. Rev.*, 2017, **117**(19), 12475–12531.
56 P. A. Wright, *Microporous Framework Solids*, RSC Publishing, Cambridge, 2008.
57 S. Xin, *et al.*, The acidic nature of "NMR-invisible" tri-coordinated framework aluminum species in zeolites, *Chem. Sci.*, 2019, **10**, 10159–10169.
58 Q. Zhao, W.-H. Chen, S.-J. Huang, Y.-C. Wu, H.-K. Lee and S.-B. Liu, Discernment and quantification of internal and external acid sites on zeolites, *J. Phys. Chem. B*, 2002, **106**, 4462–4469.
59 I. Wolf, H. Gies and C. A. Fyfe, Ordering of Silicate Layers by Hydrogen-Bonding Networks: Solid State NMR Investigation of the Perfect Three-Dimensional Registration in the Layer Silicate RUB-18, *J. Phys. Chem. B*, 1999, **103**, 5933–5938.
60 M. Borowski, I. Wolf and H. Gies, Investigation of Proton Dynamics within the Hydrogen-Bond Network of the Layer Silicate Na-RUB-18, *Chem. Mater.*, 2002, **14**, 38–43.
61 Q. Zhao, W. Chen, S. Huang, Y. Wu, H. Lee and S. Liu, Discernment and Quantification of Internal and External Acid Sites on Zeolites, *J. Phys. Chem. B*, 2002, **106**(17), 4462–4469.
62 R. Zhao, Z. Zhao, S. Li and W. Zhang, Insights into the Correlation of Aluminum Distribution and Brönsted Acidity in H-Beta Zeolites from Solid-State NMR Spectroscopy and DFT Calculations, *J. Phys. Chem. Lett.*, 2017, **8**(10), 2323–2327.
63 C. Bornes, C. F. G. C. Geraldes, J. Rocha and L. Mafra, Investigating trimethylphosphine oxide interactions with Brønsted and Lewis acid sites in zeolites: A comparative solid-state NMR study of wet-phase and gas-phase adsorption techniques, *Microporous Mesoporous Mater.*, 2023, **360**, 112666.
64 C. Bornes, D. Stosic, C. F. G. C. Geraldes, S. Mintova, J. Rocha and L. Mafra, Elucidating the Nature of the External Acid Sites of ZSM-5 Zeolites Using NMR Probe Molecules, *Chem. – Eur. J.*, 2022, **28**, e202201795.
65 K. Chen, S. Horstmeier, V. T. Nguyen, B. Wang, S. P. Crossley, T. Pham, Z. Gan, I. Hung and J. L. White, Structure and Catalytic Characterization of a Second Framework Al(IV) Site in Zeolite Catalysts Revealed by NMR at 35.2 T, *J. Am. Chem. Soc.*, 2020, **142**(16), 7514–7523.
66 K. Chen, Z. Gan, S. Horstmeier and J. L. White, Distribution of Aluminum Species in Zeolite Catalysts: ^{27}Al NMR of Framework, Partially-Coordinated Framework, and Non-Framework Moieties, *J. Am. Chem. Soc.*, 2021, **143**, 6669–6680.
67 K. Chen, A. Zornes, V. Nguyen, B. Wang, Z. Gan, S. P. Crossley and J. L. White, ^{17}O Labeling Reveals Paired Active Sites in Zeolite Catalysts, *J. Am. Chem. Soc.*, 2022, **144**, 16916–16929.
68 K. Chen, M. Abdolrhamani, E. Sheets, J. Freeman, G. Ward and J. L. White, Direct Detection of Multiple Acidic Proton Sites in Zeolite HZSM-5, *J. Am. Chem. Soc.*, 2017, **139**, 18698–18704.

69 G. C. Pimentel and A. L. McClellan, *The Hydrogen Bond*, W. H. Freeman, trade distributor, Reinhold Publishing Corporation, New York, 1960.
70 D. Song, S. An, Y. Sun and Y. Guo, Efficient conversion of levulinic acid or furfuryl alcohol into alkyl levulinates catalyzed by heteropoly acid and ZrO_2 bifunctionalized organosilica nanotubes, *J. Catal.*, 2016, **333**, 184–199.
71 C. R. Patil, S. P. Kamble and C. V. Rode, Single-Pot Alcoholysis of Furfuryl Alcohol to Alkyl Levulinates Using Heterogenized p-TSA Catalyst, *ChemistrySelect*, 2021, **6**, 6636–6643.
72 Y. Li, S. Wang, S. Fan, B. Ali, X. Lan and T. Wang, Nano-H-ZSM 5 with Short b Axis Channels as a Highly Efficient Catalyst for the Synthesis of Ethyl Levulinate from Furfuryl Alcohol, *ACS Sustainable Chem. Eng.*, 2022, **10**, 3808–3816.
73 H. Tian, Y. Shao, C. Liang, Q. Xu, L. Zhang, S. Zhang, S. Liu and X. Hu, Sulfated attapulgite for catalyzing the conversion of furfuryl alcohol to ethyl levulinate: Impacts of sulfonation on structural transformation and evolution of acidic sites on the catalyst, *Renewable Energy*, 2020, **162**, 1576–1586.
74 Y. Ma, J. Ding, L. Yang, X. Wu, Y. Gao, R. Ran and D. Weng, Flexible Al Coordination with H_2O Explaining the Deviation of Strong Acid Amount from the Framework Al Content in Al-Rich SSZ-13, *J. Phys. Chem. C*, 2023, **127**(33), 16598–16606.
75 C. Lei, A. Erlebach, F. Brivio, L. Grajciar, Z. Tošner, C. Heard and P. Nachtigall, The need for operando modelling of ^{27}Al NMR in zeolites: the effect of temperature, topology and water, *Chem. Sci.*, 2023, **14**(34), 9101.